

Research Paper

Establishing sheep as an experimental species to validate ultrasound-mediated blood-brain barrier opening for potential therapeutic interventions

Matthew Pelekanos¹, Gerhard Leinenga¹, Mostafa Odabae¹, Maryam Odabae¹, Siamak Saifzadeh², Roland Steck² and Jürgen Götze¹,✉

1. Clem Jones Centre for Ageing Dementia Research, Queensland Brain Institute, The University of Queensland, St Lucia Campus, Brisbane, QLD 4072, Australia
2. Medical Engineering Research Facility (MERF), Institute of Health and Biomedical Innovation (IHBI), Queensland University of Technology, Prince Charles Hospital Campus, Brisbane, QLD 4032

✉ Corresponding author: j.goetz@uq.edu.au

© Ivyspring International Publisher. This is an open access article distributed under the terms of the Creative Commons Attribution (CC BY-NC) license (<https://creativecommons.org/licenses/by-nc/4.0/>). See <http://ivyspring.com/terms> for full terms and conditions.

Received: 2017.09.18; Accepted: 2018.03.02; Published: 2018.04.03

Abstract

Rationale: Treating diseases of the brain such as Alzheimer's disease (AD) is challenging as the blood-brain barrier (BBB) effectively restricts access of a large number of potentially useful drugs. A potential solution to this problem is presented by therapeutic ultrasound, a novel treatment modality that can achieve transient BBB opening in species including rodents, facilitated by biologically inert microbubbles that are routinely used in a clinical setting for contrast enhancement. However, in translating rodent studies to the human brain, the presence of a thick cancellous skull that both absorbs and distorts ultrasound presents a challenge. A larger animal model that is more similar to humans is therefore required in order to establish a suitable protocol and to test devices. Here we investigated whether sheep provide such a model.

Methods: In a stepwise manner, we used a total of 12 sheep to establish a sonication protocol using a spherically focused transducer. This was assisted by *ex vivo* simulations based on CT scans to establish suitable sonication parameters. BBB opening was assessed by Evans blue staining and a range of histological tests.

Results: Here we demonstrate noninvasive microbubble-mediated BBB opening through the intact sheep skull. Our non-recovery protocol allowed for BBB opening at the base of the brain, and in areas relevant for AD, including the cortex and hippocampus. Linear time-shift invariant analysis and finite element analysis simulations were used to optimize the position of the transducer and to predict the acoustic pressure and location of the focus.

Conclusion: Our study establishes sheep as a novel animal model for ultrasound-mediated BBB opening and highlights opportunities and challenges in using this model. Moreover, as sheep develop an AD-like pathology with aging, they represent a large animal model that could potentially complement the use of non-human primates.

Key words: blood-brain barrier (BBB), large animal model, simulation, skull, therapeutic ultrasound

Introduction

Routinely used in the medical field for diagnostic imaging, ultrasound is increasingly being explored for its neuromodulatory and also therapeutic potential (either as a neurosurgical tool for tissue coagulation or for the delivery of therapeutic agents to the brain). However, the human skull presents a challenge as it consists of two layers of cortical bone and a central layer with liquid-filled

pores, which can both reflect and distort ultrasound, thereby dampening the pressure wave and heating the bone [1]. This problem has been partially addressed using phased array systems, which allow for tissue coagulation by focusing continuous high energy ultrasound waves [2,3]. In the case of drug delivery, low energy-pulsed ultrasound is being used in a protocol that involves interaction with

intravenously injected microbubbles to achieve a transient opening of the blood-brain barrier (BBB) in a process we have conveniently termed obicodilation [4]. Both simple transducer systems and more complex phased arrays have been used [5]. An alternative strategy requires craniotomy to implant a transducer in a fixed position. This circumvents the need to transmit ultrasound through the skull bone but the method also has its limitations [6]. A series of studies has been conducted to determine the most critical ultrasound parameters for BBB opening [7]. These include the acoustic pressure [8], transducer frequency [9], pulse repetition frequency [10], microbubble size [11], and pulse duration (burst duration) [10]. The mechanical index has been presented as a metric that describes the threshold for BBB opening, being proportional to peak negative pressure and inversely proportional to center frequency [12], such that lower frequencies have a lower pressure threshold for BBB opening. The time taken for BBB closure was found to be independent of the opening volume [13], and the amount of opening was reduced by breathing pure oxygen as opposed to air [14]. However, despite considerable progress, accessing the human brain to achieve therapeutic outcomes with ultrasound has remained a challenge, in terms of the treatment of large areas and overcoming the thickness of the skull and the heterogeneity of the brain itself.

Obicodilation has mostly been evaluated in rodents, which have a thin skull that does not present a major barrier for ultrasound transmission. Brain uptake has been demonstrated for MRI contrast agents [15,16], fluorescently labeled dextrans [17] and the dye Evans blue [18,19], which are normally excluded from the brain. Brain uptake of an antibody targeting amyloid plaques was shown to increase in a mouse model for Alzheimer's disease (AD) [20], and obicodilation also proved effective and safe in removing toxic protein aggregates in AD mouse models, either in combination with a therapeutic antibody [21,22], or on its own [19,22-25], with a concomitant improvement in memory [19,22,24]. More extensive safety studies, both short- and long-term, have also been performed in wild-type mice [8,10,12,26,27].

On the road to translation, the work in rodents continues to inspire research using larger animals, including dogs, miniature pigs and macaques [28-31]. Here, we established sheep (a species previously treated with ultrasound to induce thermal lesions [32]) as an experimental system for obicodilation, our rationale being that their skull is close to that of humans in regards to thickness, porosity and the curvature of the calvarium [32] (Figure 1). This

similarity also extends to the morphology of the brain, which, although smaller than that of humans, is also non-homogenous and gyrencephalic [33]. Finally, sheep can also live for at least 10 years and develop an AD-like pathology with age, further underscoring the attractiveness of this model for dementia research [34].

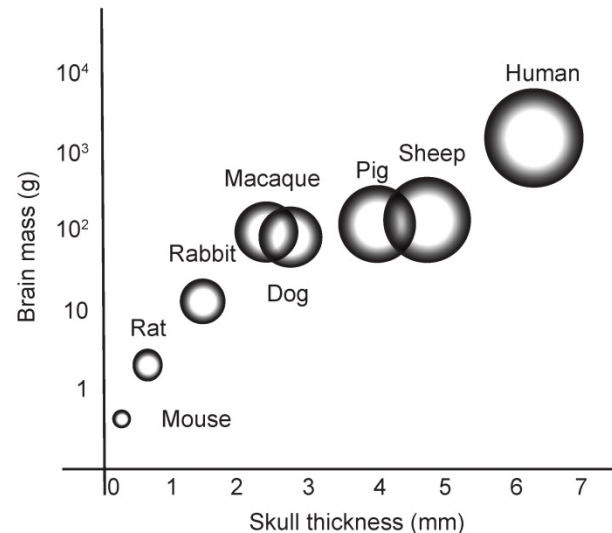


Figure 1. Brain mass versus skull thickness. Comparison of average brain mass (y-axis) and skull thickness for species currently used in ultrasound-mediated obicodilation studies.

In the current study, we developed a stepwise optimization protocol and performed *ex vivo* measurements and simulations to obtain information about focusing ultrasound through the sheep skull and the attenuation and heating that this causes. To achieve targeting of cortical areas and the hippocampus, we performed finite element analysis (FEA) simulations and successfully predicted that a 20 mm coupling cone was required to target these brain areas. We anticipate that our study will guide the future use of sheep in preclinical studies of ultrasound devices for the treatment of diseases of the brain.

Methods

Animal species and ethics

Twelve 3-8-year-old female Merino sheep (average age: 6.75 years, average weight: 54.5 kg) were used in this study (Table 1), which was approved by the Animal Ethics Committee of the Queensland University of Technology (QUT ethics approval # 1500000509) and ratified by the University of Queensland.

In vivo sonication procedure and dissection of sheep brain and skull

A flowchart of the procedure is provided in Figure S1. The sheep were positioned in sternal

recumbency on a surgical trolley and ventilated throughout the procedure with 2-2.5% isoflurane and 30% oxygen, on 10 breaths/min, and with a tidal volume of 500 mL. Anesthesia was introduced with propofol (4 mg/kg, i.v.; Provive, Claris Lifesciences Australia, Sydney, Australia) and maintained with isoflurane (IsoFlo, Zoetis, Parsippany-Troy Hills, NJ). Jugular vein cannulation was used to allow for the administration of the microbubbles and Evans blue dye. Prior to sonication, the sheep's head was shaved and fully depilated using Veet hair removal cream (Veet, Reckitt Benckiser, Slough, UK).

A spherically focused high-intensity focused ultrasound (HIFU) transducer was then positioned on the head using a coupling cone or placed directly onto the skull (**Figure 2A-B**). Ultrasound gel was applied to ensure good coupling. The sheep were sonicated in the presence of microbubbles using different parameters (**Table 1**), with a sonication time of 2 min per location (**Figure 2C**). Prior to injection, Definity microbubbles (Lantheus Medical Imaging, North Billerica, MA) were prepared and drawn into a syringe with a venting needle. Each bolus was administered at a clinical dose of 0.01 mL/kg body weight by injection into the jugular vein catheter, followed by a 5 mL saline flush and then immediate sonication. Note: custom-made microbubbles and continuous injection were initially explored, but then replaced by Definity microbubbles and bolus injections. A minimum of 5 min was allowed between multiple sonications for the microbubbles from the previous injection to mostly clear, as previously reported in beagles [31]. The mean half-life of Definity microbubbles is 1.3 min (according to product insert).

Evans blue dye (4% in saline) was administered immediately after the final sonication at a dose of 1.2 mL/kg body weight, delivered with a syringe pump at a rate of 150 mL/h over 20 min. The total time from the first microbubble injection to initiating Evans blue infusion was approximately 30 min. The sheep were then euthanized using sodium pentobarbitone (Lethabarb, 100 mg/kg; Virbac Australia, Sydney, Australia). To prevent blood clotting, heparin (250 IU/kg, i.v.; Pfizer Australia, Sydney, Australia) was given during the subsequent perfusion of saline and formalin through the carotid arteries and dissection of the brain.

After euthanasia, the sheep were decapitated and their heads flushed and perfused using administration sets ('drips') tied into the carotid arteries. Each carotid received two liters of saline flush, followed by one liter of 10% neutral-buffered formalin, delivered at a maximum drip rate. Once perfused, the brain was excised in one piece. First, the scalp was removed whole with a scalpel. Guide cuts

were then made around the calvarium in an octagonal pattern using a cordless multi-tool (18V One+ multi-tool, Ryobi, Fuchu, Japan), after which plunge cuts were driven into the guides using a surgical bone saw (System 5 Sagittal Saw, Stryker, Kalamazoo, USA). Once the plunge cuts were sufficiently deep, a surgical chisel was used to separate any remaining connections between the calvarium and the skull, and to prise up the calvarium for removal in an octagonal pattern (**Figure 2D**). Once exposed, the brain was removed by inverting the head and applying gentle pressure with a finger through the foramen magnum (**Figure 2E**). The brain and calvarium were all post-fixed in 10% formalin overnight. The next day, the brain was sectioned coronally into 7 mm blocks using a house-made brain block (**Figure 2F**). The blocks were then again post-fixed in 10% formalin overnight, after which the tissue was stored in phosphate-buffered saline (PBS) containing 0.01% sodium azide.

Computed tomography scanning

For sheep 9-12, *in vivo* CT scanning of the head was performed after sonication and Evans blue infusion, but before euthanasia. While still anesthetized, the sheep were transferred to a CT scanner (Aquilon Lightning, Canon Medical Systems, Sydney, Australia), and scanned at 120 kV and 112 mA, with a field of view of 220 mm, slice thickness 1 mm, pixel size 0.43 mm and matrix 512x512.

Ultrasound generation *in vivo*

For the sheep study, pulses were generated with a function generator (Trueform 33512B, Keysight, Santa Rosa, CA), and amplified by 50 dB using a class A linear amplifier (240L Broadband Power Amplifier, Electronics & Innovation, Rochester, NY). Two different spherically focused HIFU transducers (H-107 at 500 kHz and H-117 at 286 kHz center frequency; f-number: 1, radius: 64 mm with a 20 mm central hole; Sonic Concepts, Bothell, WA) were used and driven at a range of voltages through an impedance matching network. The ultrasound parameters for the sheep procedures are shown in **Table 1**.

Acoustic pressure mapping

To perform acoustic measurements, an Onda AIMS III tank (Onda, Sunnyvale, CA) equipped with a calibrated needle hydrophone (HNR-500, Onda) and a 20 dB preamplifier (AH-2010, Onda) was used. A H-117 transducer was driven at 286 kHz, with 1 ms pulses, at 80 V, and a pulse repetition frequency (PRF) of 20 Hz.

Simulation of ultrasound acoustic response (UAR) analysis and experimental validation

Linear time-shift invariant (LTI) systems investigate the response of a linear and time-invariant system to an arbitrary input signal. The behavior of the system is described by the mathematical expression of a 'system transfer function'. Provided that the input and transfer function are known, the output can be calculated.

Ultrasound propagation can be represented by an LTI system; the trajectories of these systems can be tracked as they move through time. We recently introduced the concept of the ultrasound acoustic response (UAR) to determine how the geometry and material of bone phantoms affect the acoustic response, extending previous work that determined the transit time spectra (TTS) of ultrasound [35]. We grouped the pre-amplifier, hydrophone and HIFU transducer as an LTI system, used the excitation voltage generated by a waveform generator as input, and generated the measured voltage as output, determining the acoustic measurement versus time, captured by a hydrophone.

We were able to estimate the impact of the skull on the attenuation and delay of ultrasound waves using UAR (analyzed with MatLab software (The MathWorks Inc., Natick, MA) doing a Wiener deconvolution) [36,37]. Measurements were taken in the AIMS III tank using a needle hydrophone (HNR-500), comparing the signals recorded in the presence and absence of a sheep skull. The amplified received signal was sent to a data acquisition platform, which included a 16-bit high speed digitizer with 250 MS/s and 14 bit resolution (Spectrum, M4i platform), supported by the SBench 6 software (Spectrum, <http://spectrum-instrumentation.com/en/sbench-6-overview>).

Simulation in ANSYS

Finite element analysis (FEA) models a wide range of physical systems [38,39]. The ANSYS software (ANSYS® Academic Research, Release 17.2, Help System, ANSYS, Inc.) [40] was used with the FEA method to model acoustic waves transmitted from a HIFU and focused in the sheep brain, thereby estimating attenuation.

These analyses compute a finite elements dynamic matrix equation: $[MF]\{\ddot{x}_e\} + [KF]\{x_e\} = \{f_F\}$ where $[M_F]$ and $[K_F]$ are the equivalent fluid mass and stiffness matrices for the system, respectively, $\{f_F\}$ is an external excitation vector in the acoustic fluid, $\{p_e\}$ is a vector of unknown nodal acoustic pressure, and $\{\ddot{p}_e\}$ is a vector of the second derivative of acoustic pressure with respect to time [40].

First, sheep skulls were scanned by CT (1 mm resolution) to create a 3D geometry of the skull cap (Figure 3A). The surface geometry, represented by triangle meshes, was simplified by 2 mm meshes to reduce the geometric complexity in the simulation (Figure 3B). The geometries of both the skull cap and the transducer were imported into the simulation domain to define the position of the transducer considering the distance and tilting angles relative to the skull cap according to preplanned sonication spots (Figure 3C).

For the simulations, a speed of sound in the skull of 2,500 m/s (mean value using 2.25 MHz immersion transducers (Olympus) based on a previously described method [41], variation of 10%), and a density of 1,710 kg/m³ were used (variation of 10%) as measured by obtaining weight/volume for 5 skull specimens. Density was determined based on water displacement and mass measurement. The computational domain contained the skull cap (applying the average values for sound speed and density), submerged in a hemispherical volume of water (speed of sound: 1,500 m/s, density: 1,000 kg/m³), and the active surface of the transducer.

The 3D geometry was then subdivided into a number of small subdomains (elements), each having a defined shape and number of nodes. The element size needed to be fine enough to reasonably resolve the wave propagation models. A general recommendation that was taken into consideration was to generate 6-20 elements per dominant wavelength along the direction of the wave [39]. A mesh convergence study was conducted in the water domain while the maximum pressure in the domain was monitored. The maximum pressure remained stable as the mesh size was reduced from 0.87 to 0.65 mm (Table S1). Therefore, at a frequency of 286 kHz, the element size in water was 0.87 mm, with the length of 6 elements equaling the wavelength in water. The same strategy was applied to the skull domain, where the element size was found to be 1.45 mm.

The excitation source was defined as an acoustic normal surface velocity at the surface curvature of the transducer, with a continuous wave propagation and at a 286 kHz frequency (Figure 3D). The vibrating surface causes acoustic particles adjacent to the surface to move, generating acoustic pressure. For purely acoustic phenomena, an acoustic contact is given as the interface between the skull and water. Note that no fluid-solid interface was defined between the skull and water as we assumed negligible displacement and deformation of the structure. To absorb outgoing acoustic waves from the computational domain, an acoustic radiation

boundary was applied to the exterior faces of the water domain [39] (Figure 3E).

Thermometry

Thermometry was performed in a Perspex tank (260x160x160 mm) on three fixed sheep calvaria. The transducer was fixed on a plate in the bottom of the tank, facing up. Thermal measurements were taken either with the skull placed on the transducer radiating face, or at a distance of 43 mm with a coupling cone. Coupling was done with degassed water, filling the tank as little as possible such that the transducer was fully submerged but the skull only contacted the meniscus of the water surface. This allowed for an even coupling while minimizing possible cooling of the skull sample by the water. The transducer settings were the same as those used successfully in sheep 5, 7 and 8 (286 kHz, 1.4 MPa peak negative pressure, 1 ms pulse duration, 2 Hz PRF). The temperature rise in the skull was measured using a thermal camera (TrueIR, Keysight), fixed on a retort stand 70 cm above the skull. Images were captured at a rate of 1/s, and the maximum temperature within a target box was recorded. External temperatures were measured using T-type thermocouples (diameter 600 μm) and a thermometer datalogger (EA15 system using EasyView 15 software, ExTech Instruments, Nashua, NH). The thermocouple was positioned with its stiff wire screwed into the HIFU holder, protruding through the central hole of the HIFU at the correct length to touch the skull surface. The testing apparatus was shielded from air currents with a large cardboard box, and allowed to equilibrate for 30 min between tests.

Macroscopic analysis

For the macroscopic analysis of the extravasation of Evans blue, the brain was coronally sliced and fixed in neutral-buffered formalin and a true color scan was conducted using a desktop photo scanner (V370 Photo, Epson, Suwa, Japan). Petechiae were counted in brains from six sheep. They were defined as blood spots <3 mm wide with indistinct edges. Those with defined edges, or following the distinct course of a blood vessel (characteristic of incomplete perfusion leaving unflushed blood vessels), were not counted. A 700 nm (far-red) scan of each brain section was done using a fluorescence scanner (Odyssey Fc, LI-COR, Lincoln, NE) for 2 min. Treated areas were delineated on each brain slice, as well as three untreated slices from each brain (slices 1-3 counting rostral to caudal), and the maximum far-red intensity for each area was recorded.

Histological analysis

Several histological methods were employed. For whole-slice analysis, brain blocks were cryoprotected in 30% sucrose in PBS and sectioned at 50 μm on a freezing microtome.

For endogenous IgG labeling, slices were antigen-retrieved in a 3% sodium lauryl sulfate/2.58% sodium citrate solution at 37 °C for 30 min, washed once with water and then 3 times for 5 min in PBS. Next, endogenous peroxidases were quenched by washing in a 3% hydrogen peroxide (in PBS) solution for 15 min. The slices were then washed again (3x 5 min PBS), blocked with 0.5% bovine serum albumin for 1 h, and incubated overnight with horseradish peroxidase-conjugated donkey anti-sheep IgG antibody (A3415, Sigma, St Louis, USA) at a 1:500 dilution. As a negative control, the antibody was omitted. The slices were subsequently washed three times in PBS, before developing in Dako DAB+ chromogen substrate (Agilent, Santa Clara, USA) according to the manufacturer's instructions. The slices were then rinsed of excess chromogen three times in PBS before being mounted whole onto chrome-alum gelatin-coated slides (ProSciTech, Townsville, Australia), and dried.

The mounted slices were defatted with multiple 5 min washes of water, ethanol, and xylene (2x tap water, 70% ethanol, 2x 100% ethanol, 2x xylene, reverse back into water), then stained with cresyl violet solution (0.1% cresyl violet acetate in 1 M sodium acetate, 2% glacial acetic acid) and rinsed thoroughly. They were then dehydrated and cleared (water-xylene, as above), and coverslip mounted with DPX mountant (Thermo Fisher, Sydney, Australia).

For region of interest analysis, Evans blue-stained pieces from sheep 10-12 were excised and paraffin embedded and then sectioned at 7 μm thickness. Sections 35 μm apart were defatted and rehydrated, and stained with either hematoxylin and eosin (H&E) or vanadium acid fuchsin (VAF) stain to assess cell damage and red blood cell infiltration. After staining, slides were cleared and mounted as above. To further confirm IgG extravasation, fluorescent lectin/IgG co-labeling was performed. Rehydrated sections were antigen retrieved, blocked, and incubated with lectin biotin conjugate (Sigma) at 1:250 overnight, washed and then incubated with 1:500 dilutions of streptavidin conjugated alexa-555 and anti-sheep IgG-488 (Life Technologies, Carlsbad, USA) for 2 h. Slides were imaged for fluorescence on a Discovery spinning-disk confocal microscope (BioVision Technologies, Exton, USA), in bright field on an AxioImager microscope (Zeiss Australia, Sydney, Australia), and scanned on a slide scanner (Metafer4, Zeiss Australia, Sydney, Australia).

Table 1. Summary of sheep sonications

Sheep #	1	2	3	4	5	6
Frequency (kHz)	500	500	500	500	515 ^b	286
Sonications (#)	5	6	4	5	2	3 ^c
Pressure (MPa)	0.6-2.4	2.4	2.4	2.4	1-1.4	1.4
Pulse duration (ms)	10	10	10	10	1	10
PRF (Hz)	2	2	2	2	2	2
Microbubble type	in-house	in-house	Definity	Definity	Definity	Definity
Microbubble administration	infusion	bolus	bolus	bolus	bolus	bolus
Evans blue administration (delay/min)	10	10	10	10	immediate	immediate
Evans blue-positivity ^a	-	-	-	-	N.A.	+ ^a
Sheep #	7	8	9	10	11	12
Frequency (kHz)	286	286	286	286	286	286
Sonications (#)	5	5	4	11	5	5
Pressure (MPa)	1.4	1.4	1.4-2.4	1.4-2.4	1.4-2.4	1.4-2.4
Pulse duration (ms)	1	1	1	1	1	1
PRF (Hz)	2	2	2	2	2	2
Microbubble type	Definity	Definity	Definity	Definity	Definity	Definity
Microbubble administration	bolus	bolus	bolus	bolus	bolus	bolus
Evans blue administration (delay/min)	immediate	immediate	immediate	immediate	immediate	immediate
Evans blue-positivity ^a	+ ^a	+ ^a	N.A.	+	+	+

^aSonication spot 5 only; ^bafter a transducer recalibration, 515 instead of 500 kHz was used; ^csonication spots 1, 2 and 5; N.A., not available

Results

Study design

Our non-recovery protocol included a total of 12 sheep with on average five sonication points each, based on the use of a spherically focused HIFU transducer (**Table 1** and **Figure S1**).

In a pilot study, sheep 1-4 helped to establish the general procedures including anesthesia, sonication protocol plus microbubble administration, brain and skull dissection and the histological analysis.

Sheep 5-8 were used to establish reproducibility and efficacy in opening the BBB at the base of the brain. We also performed *ex vivo* thermometry, used CT scans to create a 3D model of the skull and performed simulations of the HIFU and skull in water (FEA and UAR analysis), followed by measuring the trans-skull acoustic pressure.

Sheep 9-12 were used to target areas that include the cortex and hippocampus (where plaque pathology concentrates in AD) using simulations and optimizations based on data obtained with sheep 5-8. We introduced *in vivo* CT imaging and were able to predict a cortical/hippocampal focus and sufficient pressure to open the BBB in the regions of interest. The simulation suggested the use of a 20 mm coupling cone, which allowed us to achieve targeted BBB opening in sheep.

BBB opening established in sheep

The first two cohorts included eight sheep in total with an average of five sonication points each (**Table 1**), either placing the transducer directly on the

skull, aimed at targeting deep, basal brain areas (**Figure 2A**), or with a 43 mm coupling cone, aimed at targeting a more shallow focus close to the skull (**Figure 2B**). The sonication spots were chosen without relying on image guidance or using stereotaxic coordinates; rather, we selected easily palpable anatomical features on the skull, which were able to stably and repeatedly accommodate the transducer assembly (**Figure 2C**).

For the first four sheep, parameters such as frequency, microbubble type and delivery, and acoustic pressure were varied before gaining consistent Evans blue staining in the brain (**Table 1**). Sheep 1 was sonicated using a 500 kHz transducer, but failed to reveal Evans blue uptake. A likely explanation was insufficient microbubble concentration in the circulation due to slow infusion. We therefore moved to bolus injections of the microbubbles from sheep 2 onwards, and from custom-made to Definity microbubbles from sheep 3 onwards. However, again we failed to achieve overt BBB opening as visualized by the absence of Evans blue extravasation. We then increased the voltage to the maximum output of the amplifier to ensure sufficient pressure. This still proved unsuccessful at producing an Evans blue signal in the brain, but as sheep 4 displayed some subdural hemorrhages at the site of sonication, it was apparent that sufficient ultrasound energy had reached the brain, but that the dye was not extravasated. As the next step, we changed the transducer to one with a lower 286 kHz frequency to obtain better skull penetration. Further, rather than having a 10 min delay between sonication

and Evans blue administration, we administered the dye immediately after the last sonication.

Successful Evans blue uptake was consistently achieved for sonication location #5 (at the base of the brain) in sheep 5-8, using a bolus injection of Definity microbubbles, 286 kHz bursts of 1 ms duration, a 1.4 MPa peak negative pressure, and a PRF of 2Hz, and either a 10 ms (sheep 6) or a 1 ms (sheep 5, 7 and 8) pulse duration. This was evident when a full anterior to posterior series of coronal brain sections was

visualized in natural color (**Figure 4A-B**), and in fluorescence images of the same slices, with Evans blue fluorescence intensity indicated in heat-map coloration (**Figure 4C-D**). A minimum of 5 min delay was allowed between sonications to allow for clearing of most of the microbubbles from the circulation. To visualize BBB opening with an alternative method, we stained sections with cresyl violet and anti-sheep IgG, revealing pronounced IgG uptake for sonication point #5 that matched the Evans blue pattern (**Figure 4E-F**).

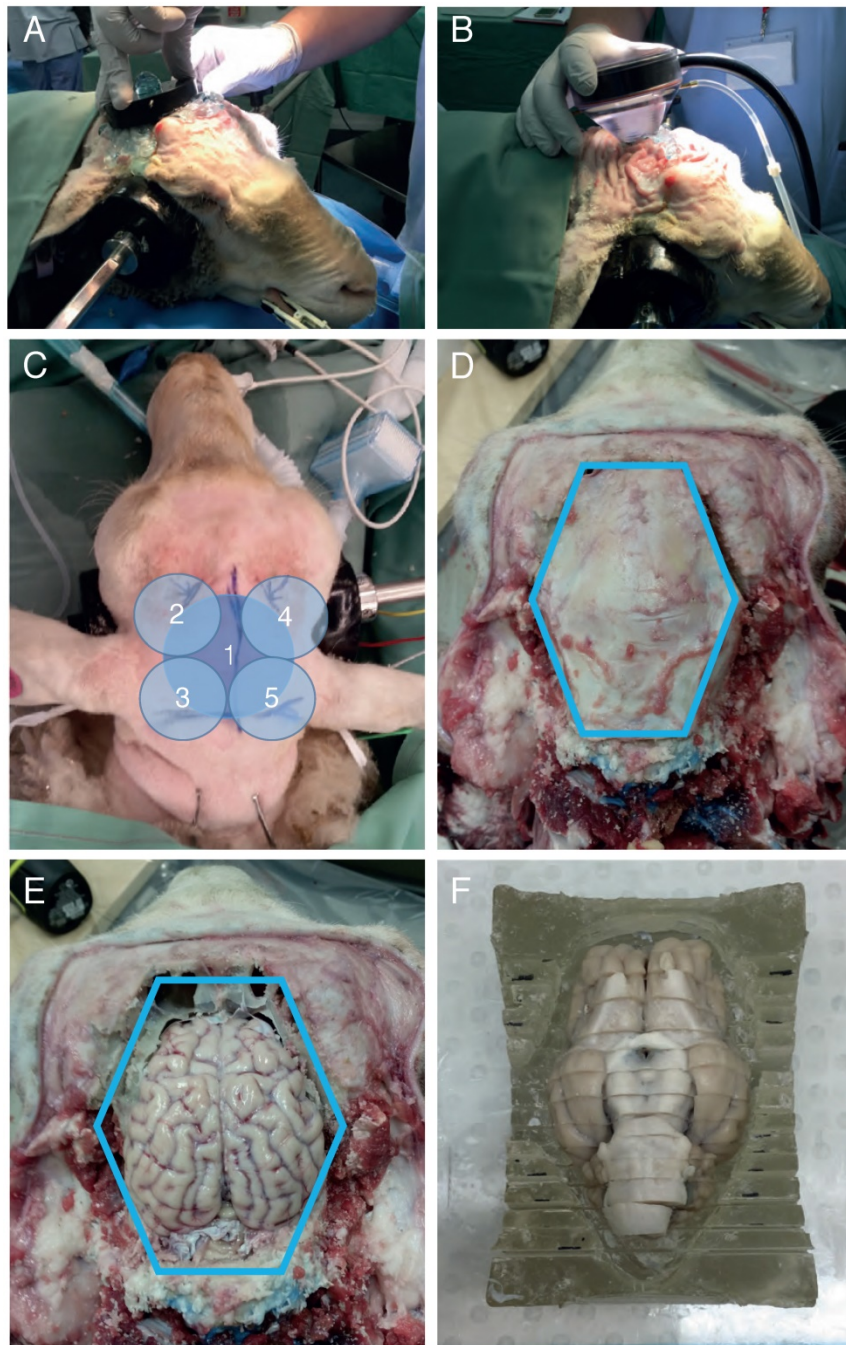


Figure 2. Sheep sonication procedure. (A) Application of a transducer directly to the sheep head without a coupling cone to provide a focus at the base of the brain. (B) Transducer application to the sheep head using a coupling cone to provide a cortical/hippocampal focus. (C) Example sonication positions. 1: with the transducer being applied directly to the head; 2-5: using a coupling cone for the transducer. (D) Illustration of the skull dissection. The blue line indicates the surgical saw cuts around the calvarium. (E) After the calvarium was removed intact for *ex vivo* testing, the brain was exposed and ready to be removed. (F) Illustration of the brain in a cutting block, having been sliced but not separated.

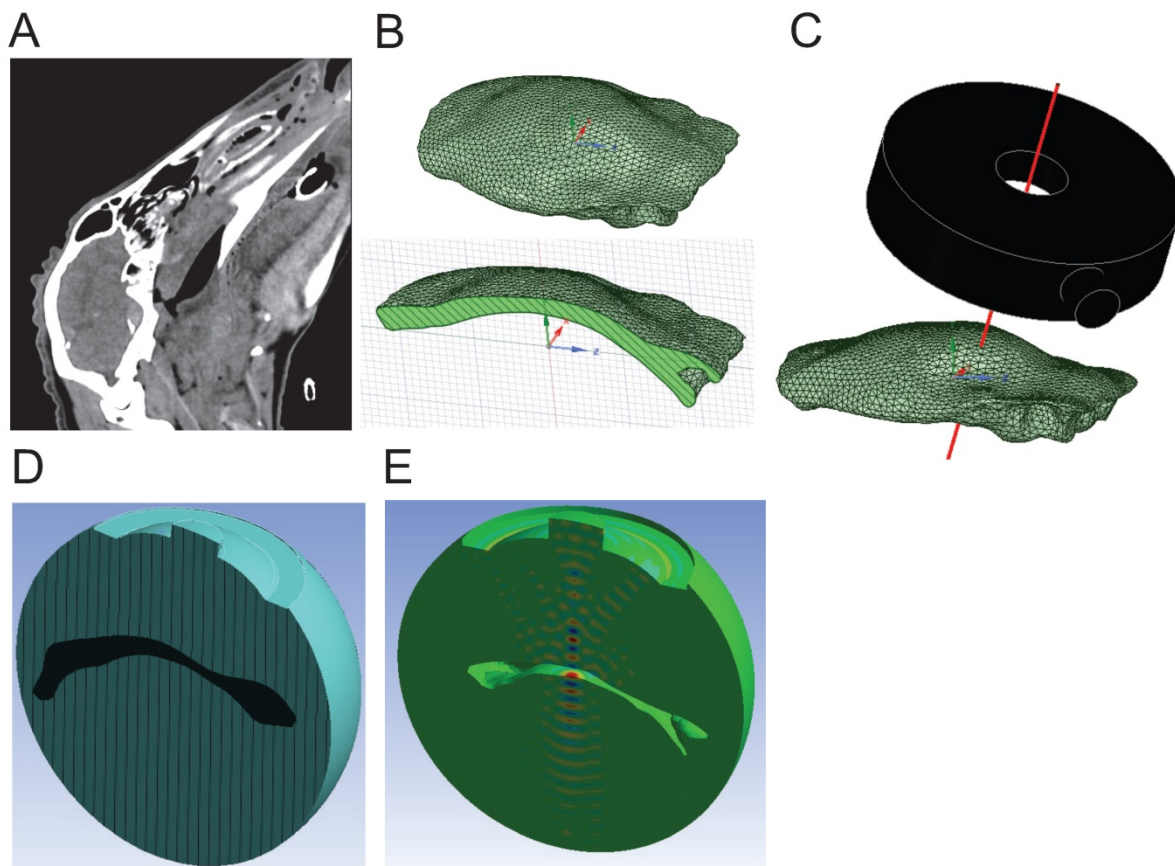


Figure 3. Simulation process from CT scan to ANSYS FEA. (A) CT scan of the sheep skull used to create the 3D model of the skull cap. (B) Full 3D geometry of the skull cap imported into ANSYS shown from above (top) and in cross-section (bottom). (C) The HIFU (black model) was precisely positioned such that the axis of the central hole (red line) was aligned with the sonication spot on the skull cap. (D) Two main domains of water (blue) and skull cap (black) were created. Note that only half of the computational domain is shown. (E) 3D pressure contour (FEA result) in the water domain. Note that the skull cap domain has been removed for better visualization.

Together, the BBB at the base of the brain was successfully opened (applying the transducer directly to the head), whereas in shallow areas (using a 43 mm cone) it was not. We next aimed to achieve targeting of hippocampal and cortical areas, assisted by simulation optimization. We anticipated that we would need a smaller coupling cone than used for shallow targeting.

Acoustic simulations to optimize *in vivo* targeting

We next performed a 3D simulation of the acoustic field of the 286 kHz HIFU in water in the absence of a skull using FEA shown as a 2D representation (Figure 5A), followed by validating the pressure distribution in an AIMS III tank filled with water, again in the absence of a skull (Figure 5B). For both the simulation and the experiment, the focal zone (maximum pressure) was 43 mm distant from the outer edge of the transducer. When the signal decay at -3 dB (about 0.75 of the maximal normalized pressure) was assessed, the only difference between the simulated and the measured data was that, for the latter, the focal zone was shifted 4 mm towards the transducer surface (Figure 5B). This was not

unexpected considering that the HIFU transducer (active diameter: 64 mm, radius of curvature: 59.97 mm, f-number = 0.93) deviated from the provided specifications (diameter: 64 mm, radius of curvature: 64 mm, nominal f-number = 1.0) (see also: [42]).

Next, 3D simulations were performed of the sheep skull cap in water (with water as a reference) using two sonication spots that were 14 mm apart (Figure 6A) to obtain a pressure map at a defined plane inside the cap (Figure 6B). The simulations were again validated in the AIMS III tank, positioning the skull cap by means of a 3D-printed holder to achieve the same position and angle as in the simulation (Figure 6C), and the pressure map was obtained at this plane. For both the simulation and experimental validation, the absolute pressure value was normalized for the maximum pressure in water in the absence of the skull cap. For both sonication spots (Figure 6D-E), the location of the maximum pressure in terms of depth and the pressure distribution were in good agreement with the simulation. This validated the FEA, which we then used to optimize the positioning of the HIFU and the targeting of the focus to reduce transmission loss.

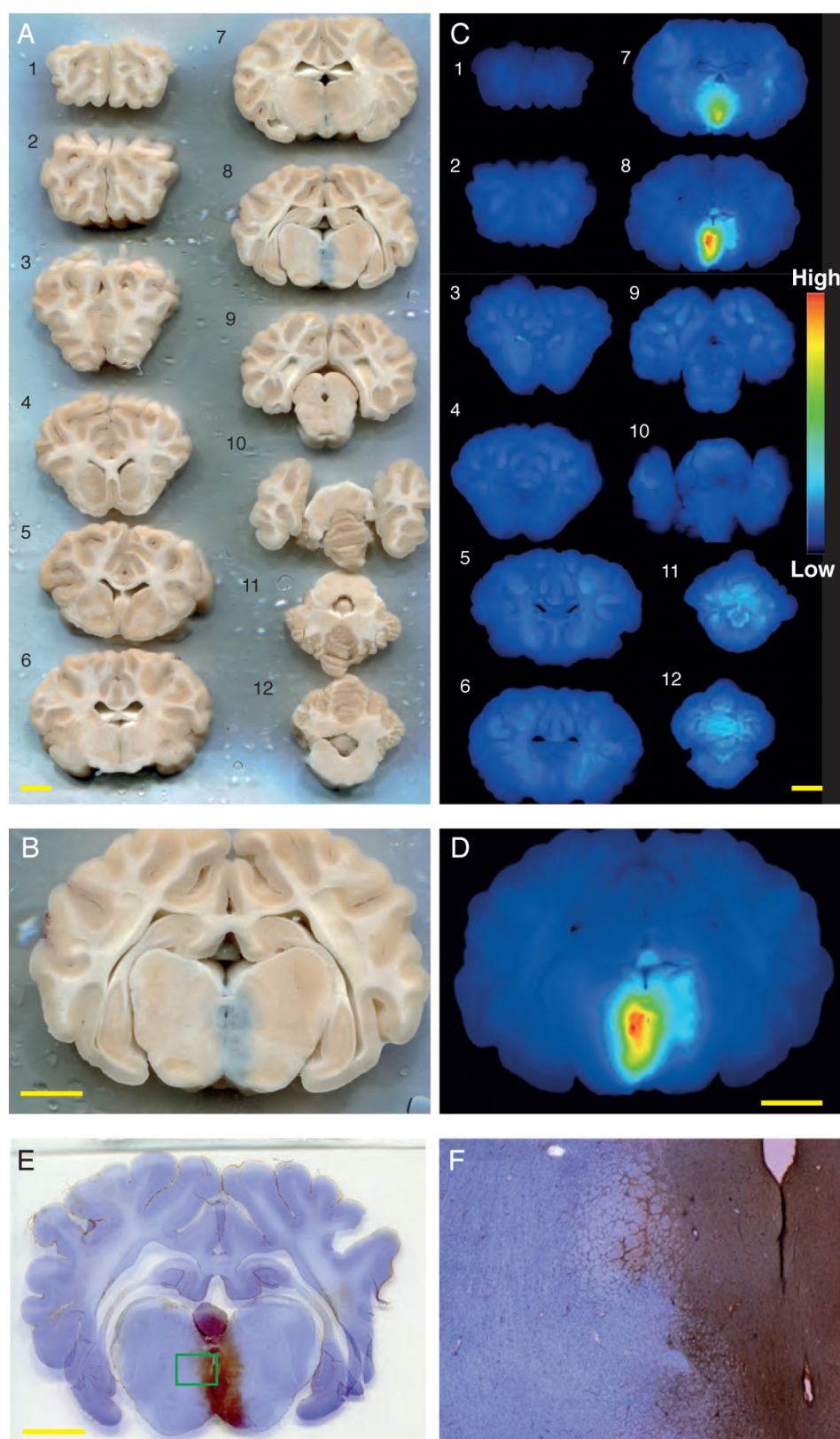


Figure 4. Obicodilation of areas at the base of the brain visualized with Evans blue. **(A)** Full series of coronally sliced brain sections (sheep 5), scanned in natural color. Evans blue uptake is seen as a blue mark in slice 8. **(B)** Close-up view of slice 8. **(C)** LI-COR fluorescence images taken of the same slices at 700 nm, demonstrating the presence of Evans blue by heat-map coloration. **(D)** LI-COR fluorescence close-up view of slice 8. **(E-F)** To visualize BBB opening with an alternative method, sections were stained with cresyl violet and anti-sheep IgG, revealing pronounced IgG uptake ((F) is inset from (E)). Scale bars: 10 mm.

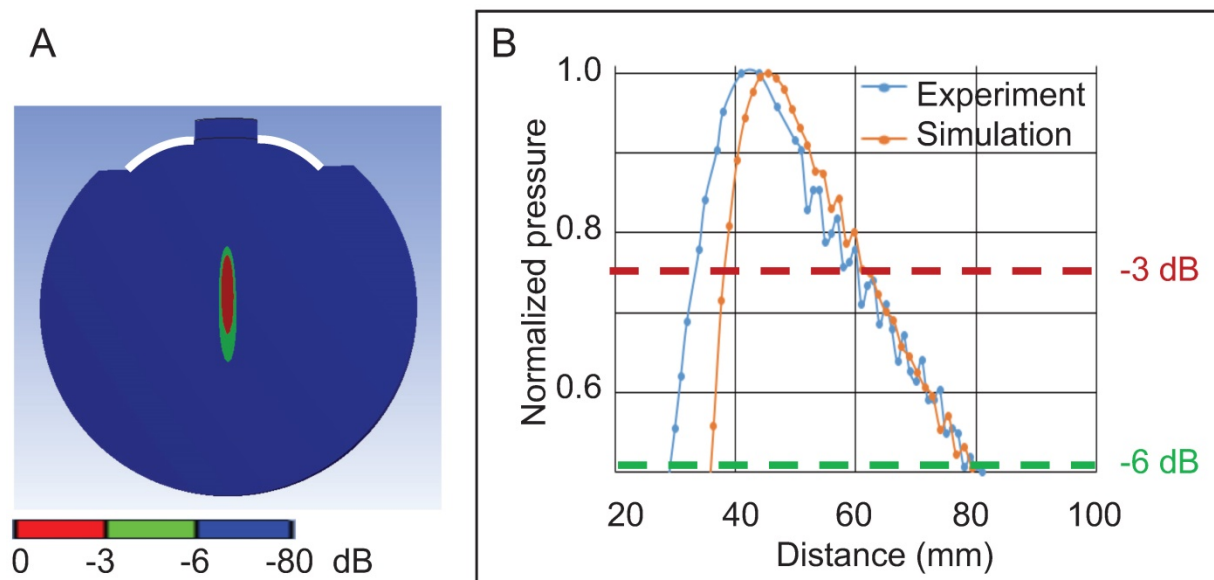


Figure 5. Validation of a 3D simulation of the 286 kHz HIFU acoustic field in water in the absence of a skull. **(A)** A 2D representation of the focus of the HIFU in water (showing the active surface of the HIFU in white). **(B)** Graph showing the normalized pressure profile in the experiment compared to the simulation as a function of the distance from the edge of the HIFU.

Two sonication spots 20 mm apart (to ensure that the spots were not overlapping) were modeled in the simulations in which the cone height (distance between the active surface of the HIFU and the skin surface) was changed from 0 mm to 40 mm in 10 mm increments. We determined that the thickness of the scalp varied between 4 mm and 5 mm, and added this distance to the simulation (Figure 7A), modeling its acoustic properties as water [43]. In the absence of a cone, the -6 dB contour was 35x6 mm at the base of the brain, and the skull base (Figure 7B). With a 10 mm cone, the -6 dB contour was reduced to 30x6 mm and the focus was repositioned axially towards the face of the transducer, overlapping the base of the brain and the hippocampus (Figure 7C). With a cone height of 20 mm, cortical and hippocampal areas were targeted within the -6 dB pressure contour of size 35x6 mm and this positioning yielded the highest focal maximal pressure of 0.7 (normalized pressure) estimating 30% attenuation caused by the sheep skull cap (Figure 7D). By increasing the cone height to 30 mm and 40 mm, the focus moved towards the face of the transducer and energy was deposited on the calvarium and outside the skull where the majority of the wave's energy was reflected by the skull cap surface (Figure 7E-F).

When establishing a pressure profile at a -6 dB pressure contour for both sonication spots (Figure 7G), the targeting area was also confirmed for spot 2, with a slightly higher pressure. One should note that for a given cone height, for the two sonication spots examined, the HIFU targeted the brain at a similar depth (with a displacement of ± 2 mm) and creating a similar focal size (variation of 4 mm) (Figure 7H). We

thus determined that the 20 mm cone was most suitable as it targeted the cortex and hippocampus, areas of interest in AD and in which the -6 dB pressure contour of the focus would provide the required pressure for opening BBB (sheep 9-12).

Predicting attenuation of the waveform by the sheep skull

To estimate how much acoustic energy reaches the brain at the focal point in cortical areas (using a 20 mm cone), we tested *ex vivo* skulls from three sheep in a test bed (Figure 8A-B), by applying a recently derived analysis, UAR. UARs in the presence or absence of a sheep skull were computed at the focal point. The UAR data in the absence (water only) and presence of a skull are shown at the cortical/hippocampal focus (Figure 8C). We always compared two adjacent peaks (with the blue line corresponding to the water condition and the red line to the skull condition), and assessed the amplitude and time delay (Figure 8D). The UAR peak time comparison revealed that the presence of the sheep skull reduced the delay of sound compared to water (because the speed of sound in the sheep skull is higher than that of water). The reduction in the delays varied between 1.16 μ s and 1.31 μ s (sheep 12), 0.8 μ s and 1.24 μ s (sheep 11), and 1.18 μ s and 1.16 μ s (sheep 10) for the focal point. We also found that the amplitude ratio of the UAR peaks varied between 30% and 50% for sheep 12, 32% and 60% for sheep 11, and 31% and 54% for sheep 10. This shows that the attenuation caused by the sheep skull cap is around 40%, 47%, and 40% on average, respectively.

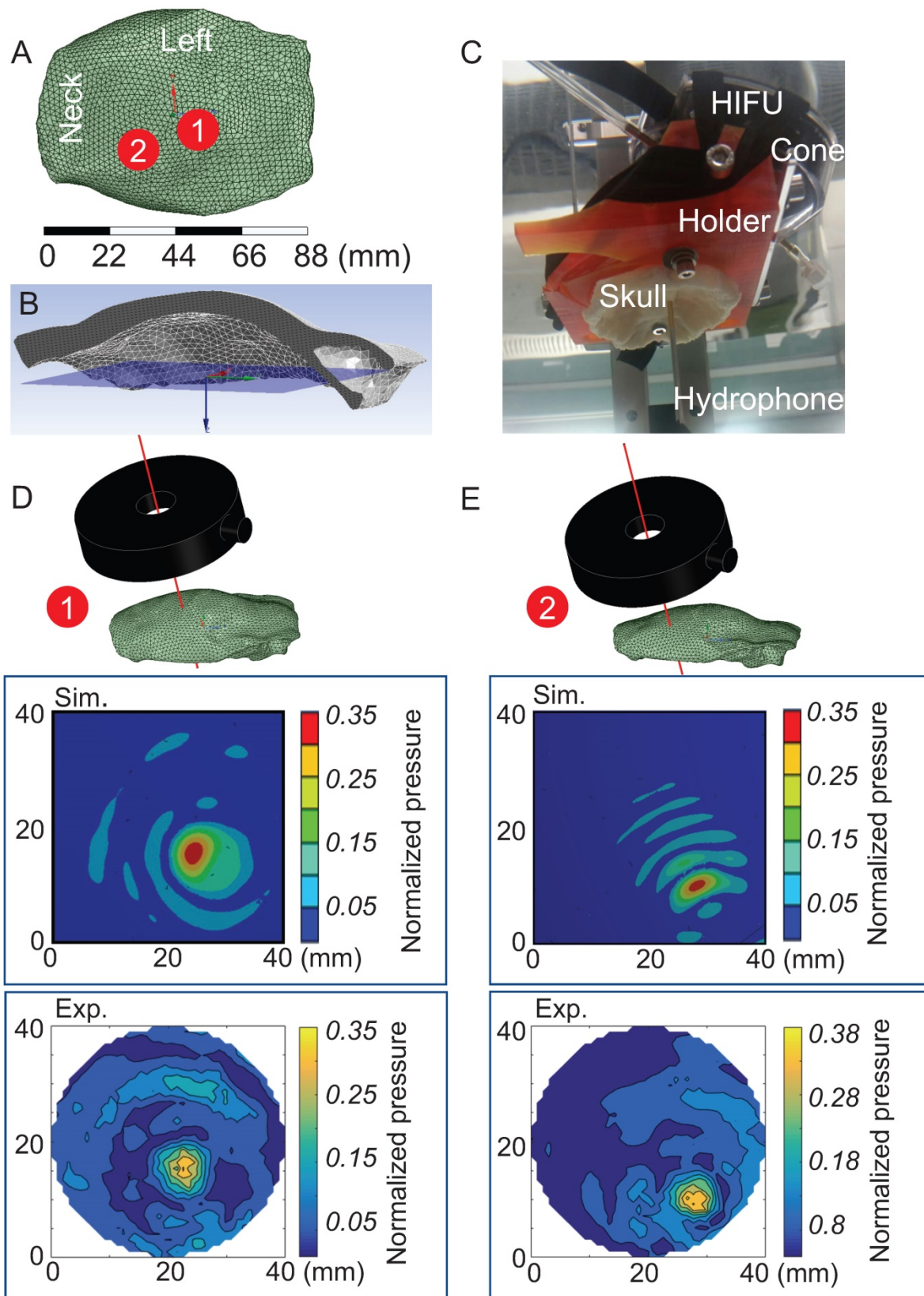


Figure 6. Validation of 3D simulations of sheep skull cap in water. (A) Two sonication spots 1 and 2 close to the center and on the right side of the cap are shown. **(B)** The pressure map location is shown by a blue surface inside the sheep skull cap in a cross-sectional view. **(C)** The skull cap and HIFU were fixed by means of a 3D printed holder in the AIMS III tank where the needle hydrophone measured the pressure inside the cap. **(D-E)** Pressure contours are presented for both the simulation (Sim.) and experiment (Exp.) at sonication spots 1 and 2.

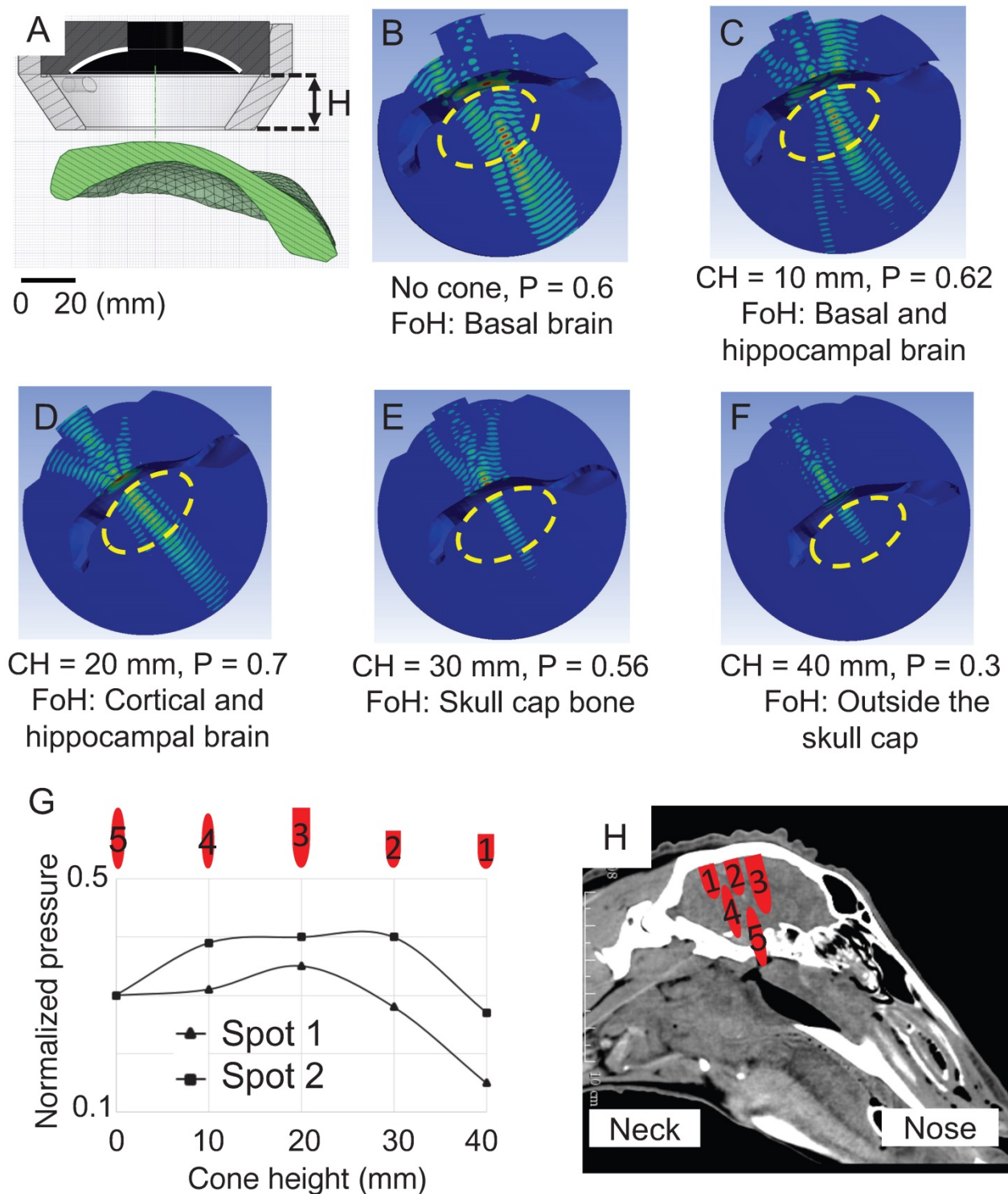


Figure 7. Optimization of the 3D simulation for two sonication spots while systematically changing the cone height. The pressure distribution in the skull bone was removed and the normalized maximal pressure was defined inside the cap. **(A)** Cross-sectional view of the HIFU, cone and skull cap. **(B)** In the absence of a cone, the normalized maximum pressure (P) inside the cap was calculated as 0.6. The focus of HIFU (FoH) was at the base of the brain. The yellow dashed oval represents the entire brain. **(C)** With a cone height of 10 mm, P was 0.62 and the focus was positioned corresponding to the base of the brain and hippocampus. **(D)** With a cone height (CH) of 20 mm, a focus was obtained in the putative cortical and hippocampal brain. **(E)** With a cone height of 30 mm, the focus was in the skull cap bone. **(F)** With a cone height of 40 mm, the focus was outside of the brain. **(G)** The normalized pressure profile of two sonication spots at the -6 dB contour is shown as a function of changing cone height. **(H)** For each cone height, the actual size of the focus is shown and registered with a CT scan of the sheep head.

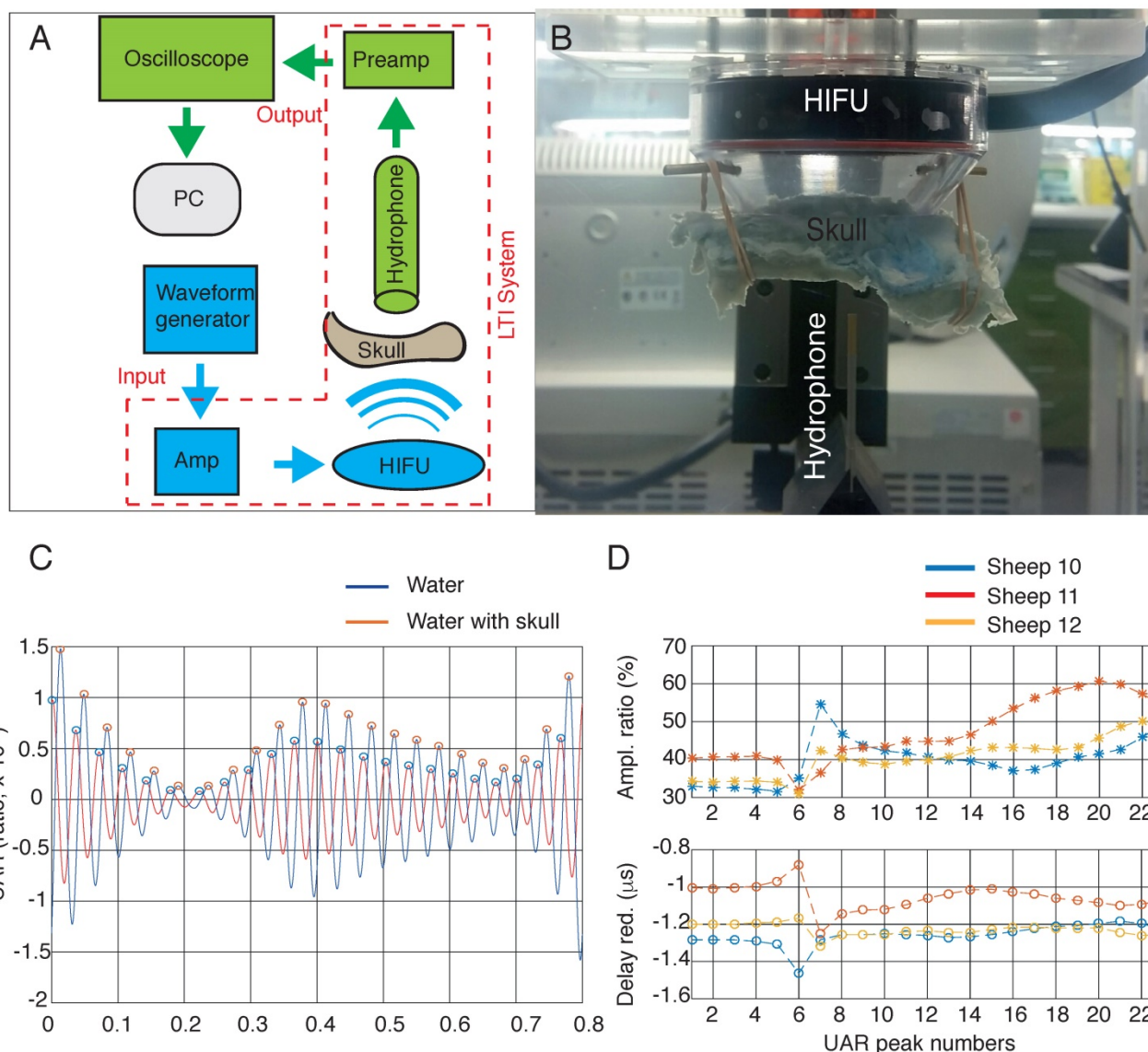


Figure 8. Attenuation. (A) Block diagram of the ultrasound test bed. The 'Transmit stream' is shown in blue, and the 'Receive stream' is shown in green. The same transmit stream is also used for the *in vivo* and thermometry experiments. (B) Experimental setup for estimating the trans-skull acoustic pressure. The HIFU transducer was placed in a holder in the Onda tank filled with degassed water. The skull was positioned with a 20 mm cone above the HIFU radiating surface, and the hydrophone sensor was positioned at the cortical focus. HIFU transducer, high intensity focused ultrasound transducer; AMP, amplifier; PC, personal computer. (C) The ultrasound acoustic response (UAR) in water and in the presence of sheep 12 skull. (D) Calculation of the amplitude ratio and the delay reduction at cortical focal points for sheep 10, 11 and 12.

Absence of significant sheep skull heating

HIFU is predominantly used for the thermal ablation of either tumor tissue or by ablating thalamic tissue in order to correct a movement disorder [44]. Tissue heating is therefore a concern and must be considered as a side-effect for any non-thermal HIFU therapy. We determined skull heating by *in vitro* thermometry, directing an infrared camera at the skull to measure its interior surface temperature, and using a thermocouple to measure its exterior temperature. Infrared images are shown after 2 min sonication with and without a coupling cone (Figure 9A-B) using the same sonication parameters that were applied to sheep 5, 7 and 8 (286 kHz frequency, 1.4 MPa peak negative pressure, 1 ms pulse duration, 2 Hz PRF).

The temperature after 2 min was recorded at the interior surface of the skull, measured with an infrared camera, and the exterior surface, measured with a thermocouple, with n=3 for all groups. Mean (\pm SD) for thermocouple measurements were as follows: baseline 21.40 °C (0.78), without cone 21.30 °C (0.46), and with cone 21.26 °C (0.40). Mean (\pm SD) for infrared measurements were as follows: baseline 21.73 °C (0.40), without cone 22.70 °C (0.50), and with cone 23.03 °C (0.06) (Figure 9C); thus, the maximum heating recorded was 1.76 °C. Assuming an average sheep body temperature of 35.70 °C, an additional 1.76 °C for two min yields a maximum temperature of 37.46 °C. Cumulative effective minutes at 43 °C (CEM43) is used to describe a thermal dose that

correlates with tissue damage [45]. In a living sheep with an average body temperature, the measured heating would result in a CEM43 of 0.0002, orders of magnitude below the lowest threshold for damage, CEM43 of 12.3, as described by McDannold and colleagues in rabbits [46].

BBB opening of cortical areas confirmed macroscopically and histologically

Considering that the HIFU generates a large focus, we aimed to achieve a pressure level at the -6 dB contour for BBB opening in a volume of 35x6 mm as estimated by FEA. According to our UAR analysis of an estimated 40% attenuation, this volume could be opened with a maximum pressure in water of 1.4 MPa resulting in 0.42 MPa in brain, 2.1 MPa in 0.63 MPa, and 2.4 MPa in 0.72 MPa, respectively.

Based on the outcome of the simulation, we used a shorter 20 mm coupling cone and a higher pressure (2.1 MPa and 2.4 MPa, the maximum achievable in

water) to open a wider area of the brain for the third cohort of four sheep, with an average of five sonication points each (Table 1). Only sheep 10-12 were further analyzed (sheep 9 was omitted for technical reasons). We achieved Evans blue staining over wide areas of the brain, including cortex and hippocampus (Figure 10A). Some of these treatments, however, also induced some hemorrhaging, particularly in white matter tracts (Figure 10B).

The analysis of petechiae in slices taken from sheep of cohorts 2 and 3 using 1 ms pulses revealed that they increased in number with sonication pressure. Unsonicated areas (control, n=9), or areas sonicated with 1.4 MPa (n=8), 2.1 MPa (n=15), and 2.4 MPa (n=19) were grouped. Mean (\pm SD) values for each group were as follows: control 0.44 (0.88), 1.4 MPa 0.63 (0.52), 2.1 MPa 5.87 (10.88), or 2.4 MPa 8.74 (9.14) (Figure 10C).

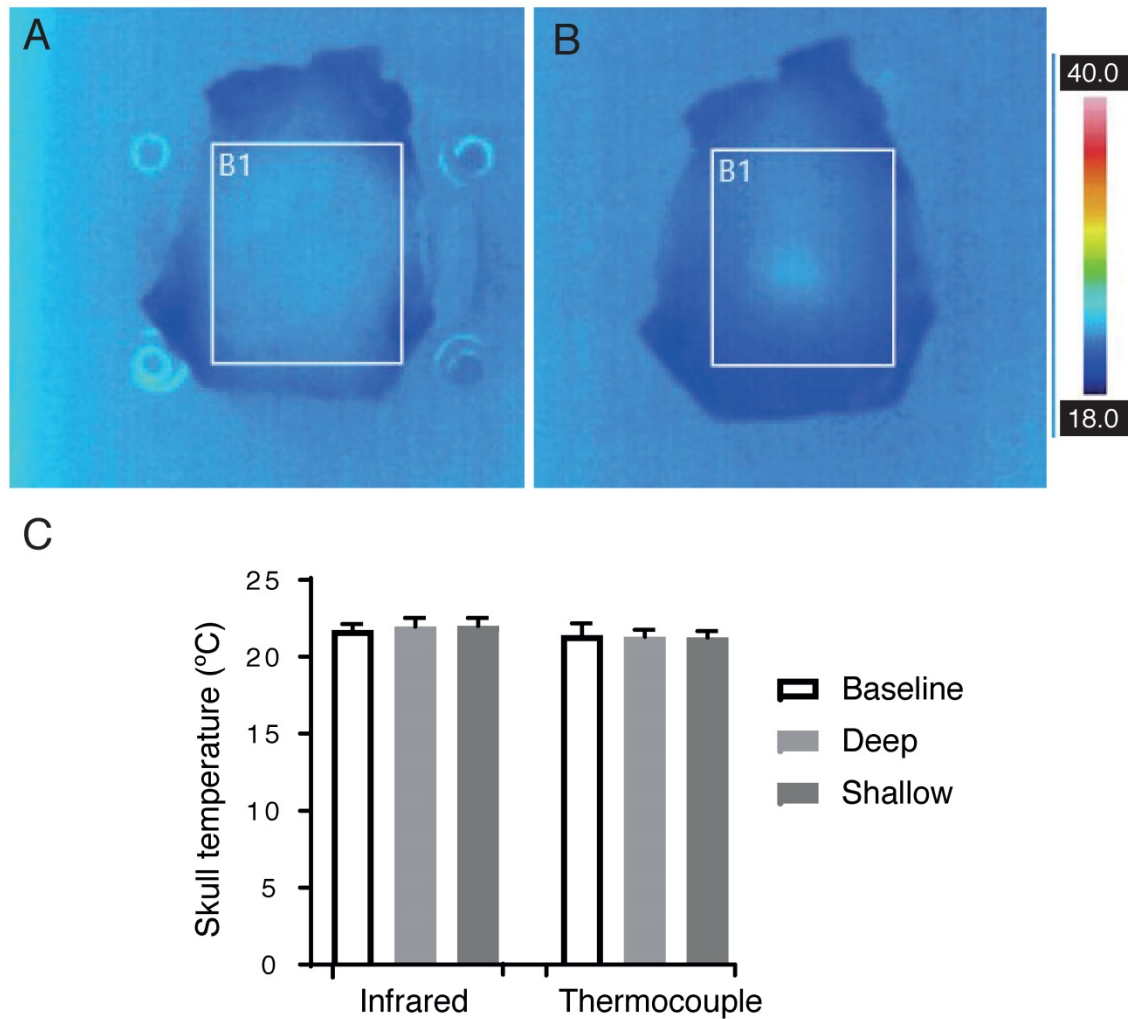


Figure 9. *In vitro* measurement of the skull bone temperature after 2 min sonication. (A-B) Infrared camera images of an ex vivo sheep skull at 286 kHz, 1.4 MPa, 1 ms, 2 Hz PRF. (A) Skull placed directly onto the transducer, and (B) using a coupling cone. (C) Mean (\pm SD) temperature measurements taken from the outer skull surface with a thermocouple, and the inner skull surface using an infrared camera (all groups, n=3).

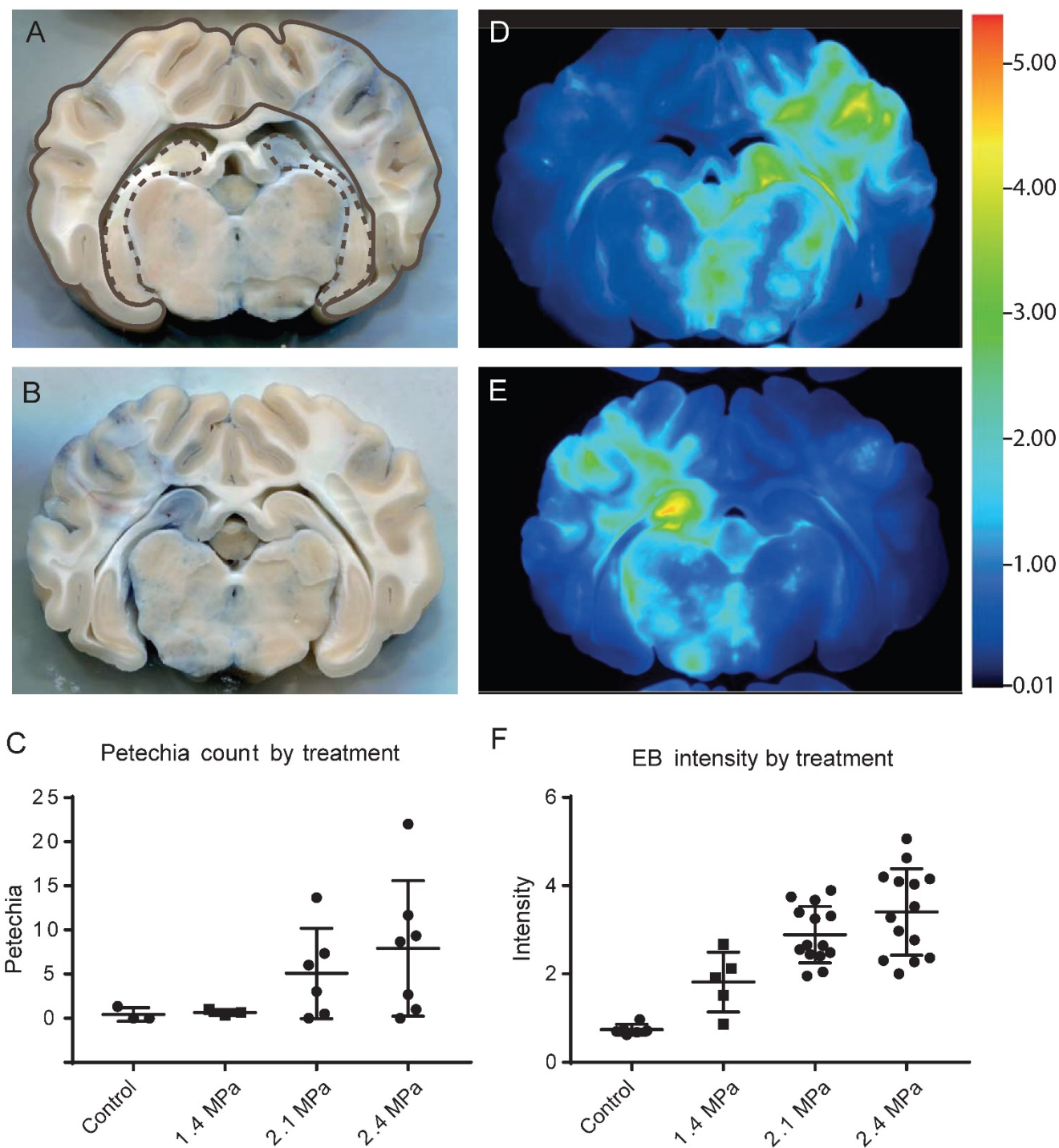


Figure 10. Analysis of Evans blue uptake in sonicated sheep brain. (A) Coronal section of fixed brain, showing extravasation primarily in cortical and hippocampal areas (top right of section). Cortical areas are delineated with a brown line and hippocampal areas with a dashed brown line. (B) Coronal section showing blue staining together with petechiae, primarily in white matter (left side of section). (C) Plot of petechia numbers within brain areas for a range of peak negative pressures. (D-E) 700 nm far-red scans of sections in A and B, with heat-map intensity coloration. (F) Plot of maximum 700 nm staining intensity in brain areas treated with 1.4, 2.1 and 2.4 MPa peak negative pressure and control.

Far-red scans also showed the extent of Evans blue extravasation throughout the brain, corresponding to the sonicated areas (Figure 10D-E). Staining intensity was quantifiable from these scans, and this increased with sonication pressure (Figure 10F). Unsonicated areas (control, n=18), or areas sonicated with 1.4 MPa (n=14), 2.1 MPa (n=41), or 2.4

MPa (n=34) were grouped. Mean (± SD) values for each group were as follows: control 0.74 (0.31), 1.4 MPa 1.88 (1.14), 2.1 MPa 3.08 (1.92), or 2.3 MPa 3.48 (1.46).

Obicodilation was also confirmed histologically. Extravasated sheep IgG provided an endogenous marker, and staining against it confirmed the

macroscopic findings of Evans blue extravasation in treated areas (**Figure 11**). Areas of BBB opening showing widespread extravasation of IgG with leakage from capillaries (**Figure 11 A, C**), whereas areas without BBB opening show little or no labeling for IgG (**Figure 11 B, D**). Cellular damage was assessed by a vanadium acid-fuchsin (VAF) stain of paraffin-embedded brain sections with only a few examples of VAF-positive (ischemic) neurons (data not shown). H&E staining was employed on paraffin-embedded brain sections to assess the presence of microhemorrhages as shown for areas

with BBB opening (**Figure 12A-D**), revealing microhemorrhages in many of the areas treated with >2 MPa and in the center of the focus, but also more peripheral large areas with BBB opening in the absence of red blood cell extravasation. Some unflushed blood vessels were also seen. Because of the size of the sheep brain and the large focal areas it was not possible to assess potential microscopic damage in a complete manner. In addition, whether these changes persist with time (beyond 1 h) has not been assessed, as the sheep underwent a non-recovery protocol.

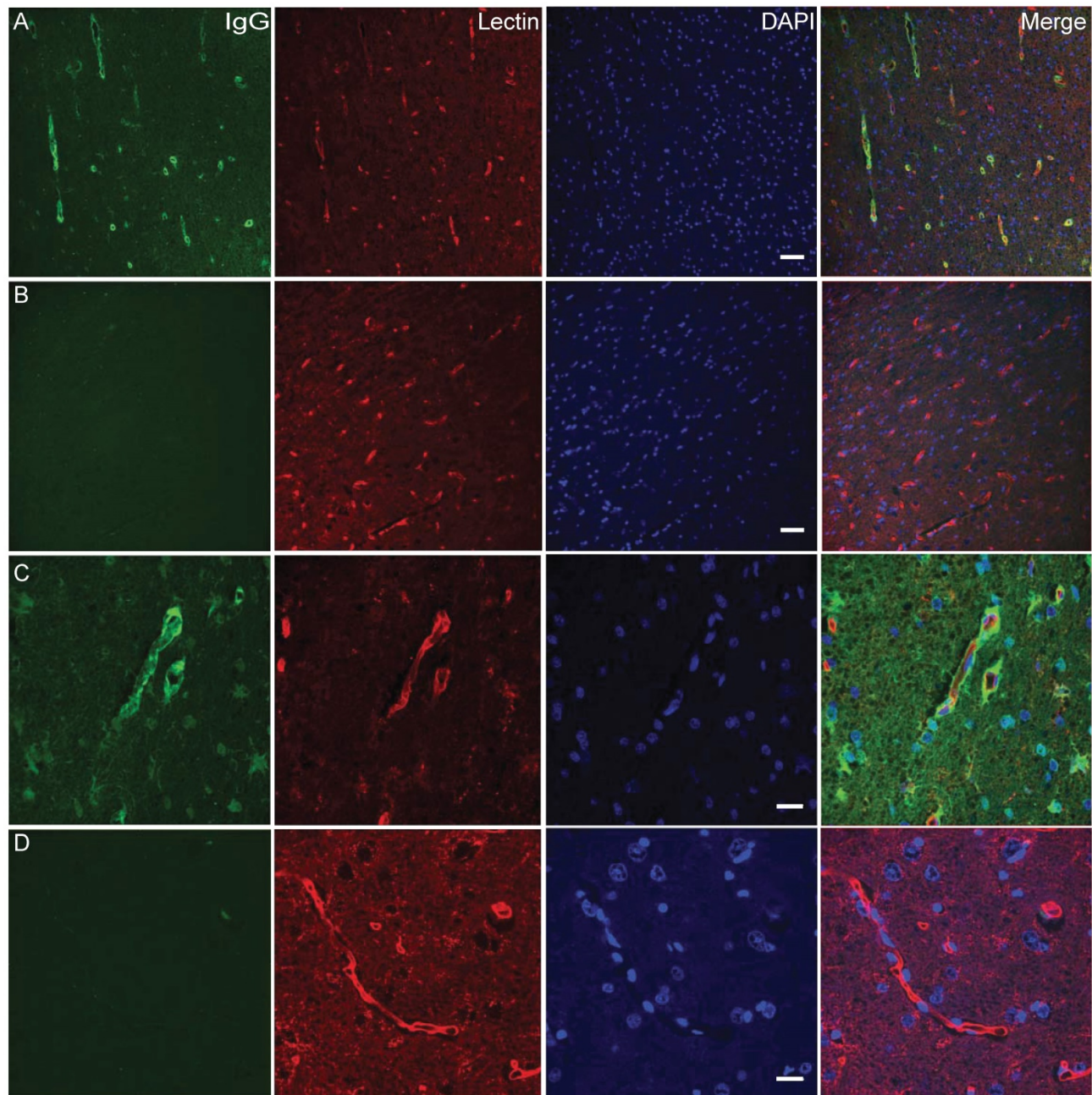


Figure 11. IgG and vasculature staining. (A, C) Area of BBB opening showing widespread extravasation of IgG (sheep IgG, in green) with leakage from capillaries (lectin staining, in red). Area without BBB opening shows little or no labeling for IgG. (B, D) High magnification imaging of leaky blood vessels in (C) showing a high concentration of IgG around vessels as well as diffusion of IgG into the brain parenchyma, as well as binding or uptake of IgG into cells. Scale bar: 20 μ m (A, C), 50 μ m (B, D).

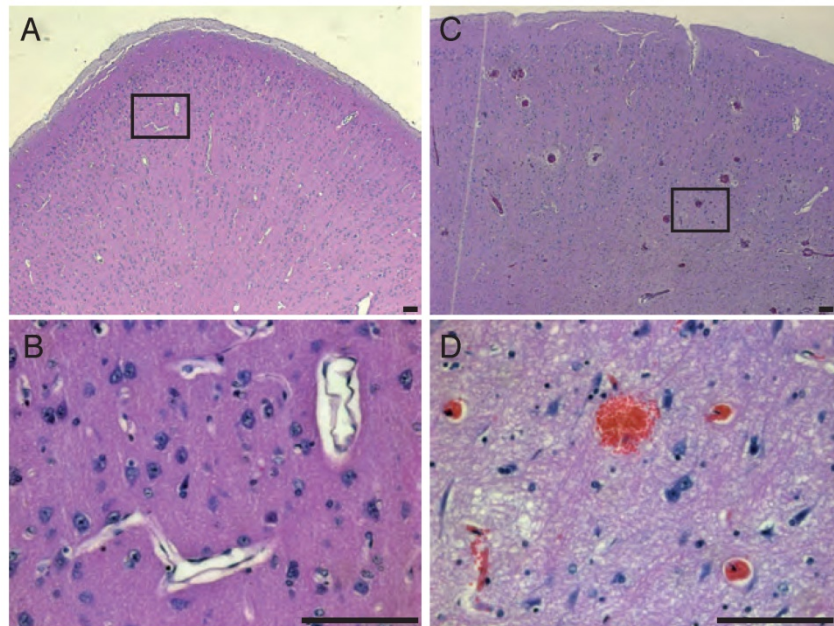


Figure 12. Hematoxylin & Eosin staining. In areas of BBB opening we detected erythrocyte extravasations by H&E staining at the focal zone when higher pressures were used (A-B). BBB opening could also be achieved without occurrence of erythrocyte extravasation as shown in (C-D). Scale bar: 100 μ m

Discussion

In the present study we have established sheep as a preclinical model for ultrasound-mediated BBB opening. We were guided by the notion that this species shares many important brain and skull features with humans. In translating rodent studies to the human setting, additional factors including body size and source (non-laboratory bred) were also considered important in order to present as many challenges to the technique as may be reasonably encountered in a clinical setting. To our knowledge, this study is the first demonstration of obicodilation in sheep, although the technique has been successfully applied in other large, complementary animals such as macaques [28,47], beagles [31] and pigs [48]. Brain size is broadly similar between these species and, unlike rodents, all have a gyrencephalic brain (Figure 1). Sheep represent an attractive model because their skull thickness and composition are similar to those of humans, they are readily available, relatively easy to use experimentally, and brain atlases are well documented for this species [49]. Sheep also have a body weight profile closer to humans and this is useful for optimizing microbubble kinetics and dosing in relation to BBB opening.

AD pathology is characterized by A β plaques and Tau tangles [50]. Of note, similar to dogs [51], sheep do naturally develop an AD-like pathology [34]. One reason may be that the A β sequence (different from rodents) is identical between sheep, dogs, pigs and humans [52], and that sequences important for Tau pathology are also conserved [34].

In order to reproduce AD pathology in rodents, transgenic mice have been generated that over-express human AD-related genes [50]. However, transgenic sheep are not available. Still, when four 8-year-old and a single 14-year-old sheep were analyzed, Tau tangle-like structures were identified in 3 of the four 8-year-old sheep, and A β -immunopositive plaques were identified in all animals, although most plaques were diffuse [34]. AD transgenic pigs have recently been generated [53], but the thickness of the pig skull continues to increase with aging [54], making this species less suitable for aged, AD, or longitudinal studies. Minipigs also possess large, air-filled sinuses atop the skull, which would block ultrasound transmission.

Macaques have the advantage that cognitive test batteries are available [29,55]. Interestingly, given that cognitive decline is a major therapeutic target in AD, a recent study used tests of executive function (discrimination learning, reversal learning and attentional set-shifting) in sheep and found that not only could they perform discrimination learning and reversals, but they could also perform the intradimensional and extradimensional set-shifting tasks that are sensitive tests of cognitive dysfunction in humans. Moreover, their performance on these shifts mirrored that seen in humans and macaques [56].

A number of different ultrasound parameters have been used successfully to open the BBB in large animals. In macaques, 500 kHz ultrasound was applied at a peak negative pressure of 250-600 kPa with a 10 ms pulse length, repeated at 2 Hz for 2 min

[57]. Also in macaques, a phased array system applied 220 kHz ultrasound with a range of peak negative pressures (223–400 kPa *in situ*) to open the BBB or to generate lesions at higher pressures [58]. In beagle dogs, 280 kHz ultrasound was applied with a peak negative pressure ranging from 1–1.2 MPa using an acoustic emissions-based controller that reduced the pressure by 50% upon detection of subharmonics. Pulse lengths of 10 ms and shorter achieved BBB opening in mice [59]. Our results demonstrate that 1 ms pulses at low frequencies suitable for trans-skull transmission (such as 286 kHz) are capable of achieving obicodilation in sheep. Shorter pulse lengths may be more advantageous than longer pulses by reducing standing wave effects [60]. PRF varied between 0.3 Hz and 10 Hz in these studies.

In the first instance, we aimed to use the HIFU transducer with a relatively large focus in order to treat larger areas of the brain, which is particularly important for diseases involving the entire brain such as AD. Thereby, the breadth of brain tissue heterogeneity including complex gyri and sulci, compartmentalized gray and white matter, and large ventricles and blood vessels is being captured [33]. These are acoustically distinct structures and it is important to account for them when refining the obicodilation technique [61]. We first aimed to target deeply situated, basal brain areas because direct transducer placement on a flat area of skull was predicted to give the best transmission of ultrasound through the skull bone. In later sheep, we used a cone of optimal height (based on simulations) of 20 mm to enhance transmission and target cortical and hippocampal brain areas, relevant to AD. Transcranial transmission reduces the effective size of the focus in which there is a tightly focused beam of high enough peak negative pressure to open the BBB. As we eventually aim to treat large areas of the brain, we enlarged the volume of sheep brain with BBB opening by generating peak negative pressures evidently above the threshold for BBB opening, which sometimes resulted in damage in the form of bleeding. Other transducer geometries should be investigated to treat a large focal area while operating below the threshold for damage. Another approach that is being pursued is to use a phased array to electronically steer the focus and sonicate each focal point sequentially using power levels calibrated by harmonic or subharmonic acoustic emissions detection. We believe sheep, due to their skull properties and large complex brains, would be a good experimental animal with which to test transducers of different geometries, volume steering by phased arrays, and acoustic emissions detection through a human-like skull.

To visualize BBB opening, we used Evans blue extravasation as done by us previously [19]. Despite this dye being a commonly used marker of BBB permeability, concerns have been raised about its appropriateness as it can exist bound to serum albumin and as a smaller unbound fraction [62]. As a complementary method, we also performed immunolabeling for sheep IgG (that is twice as large as albumin). In combining IgG with either Nissl or lectin staining, extravasation from vasculature into parenchyma was evident. Together, this demonstrated that the BBB is also penetrable for larger molecules. Other techniques that could be considered for the visualization of BBB opening include the use of fluorescently tagged dextrans of different sizes [63] or the *in vivo* measurement of the influx of gadolinium using MRI [64].

From our basic sonication protocol, it was apparent that higher peak negative pressures delivered to sheep brain resulted in increased extravasation of both Evans blue and red blood cells, the latter being potentially damaging. We found that delivering 1.4 MPa peak negative pressure gave Evans blue signal with minimal blood; however, future researchers are advised to optimise the parameters involved in the technique. Frequency and microbubble concentration being equal, pulse duration, duty cycle, PRF and peak negative pressure all affect the safety and efficacy of obicodilation.

In targeting the brain, damage of the skull and the brain in the focal area need to be avoided. Because attenuation of ultrasound can occur as a result of absorption, resulting in heating [65], we estimated the heating effects of our verified sonication parameters *in vitro*. The energy delivered due to the sonication parameters used for BBB opening was incapable of heating an *ex vivo* skull more than 2 degrees above baseline temperature, both with and without a coupling cone. It is expected that the heat dissipation measured in *ex vivo* bone is lower than *in vivo*, as reported previously [66]. This lack of heating indicates that, when using the established sonication parameters for opening the BBB, skull or tissue heating is unlikely a concern. Our study also shows when employing H&E that higher pressure was associated with erythrocyte extravasation in the center of the focus, but tissue integrity was maintained even in areas with the largest bleeds. In future studies, a recovery protocol may be included to determine long-term safety of obicodilation in sheep, and to assess tissue integrity at longer time points.

In conclusion, the thick skull bone and gyrencephalic brain of sheep presents them as a physically realistic model of obicodilation that complements the existing suite of models. This,

together with their natural AD-like aggregates in aging, positions the sheep as a clinically relevant model of obicodilation in dementia research.

Abbreviations

AD: Alzheimer's disease; BBB: blood-brain barrier; CEM43: cumulative effective minutes at 43 °C; FEA: finite element analysis; H&E: hematoxylin and eosin; HIFU: high-intensity focused ultrasound; LTI: Linear time-shift invariant; PBS: phosphate-buffered saline; TTS: transit time spectra; VAF: vanadium acid fuchsin.

Supplementary Material

Supplementary figures and tables.

<http://www.thno.org/v08p2583s1.pdf>

Acknowledgements

This study was supported by the Estate of Dr Clem Jones AO, the State Government of Queensland, the Federal Government of Australia (ACT900116), the Australian Research Council LIEF grant LE100100074, and by grants from the Australian Research Council [DP160103812] and the National Health and Medical Research Council of Australia [GNT1127999, GNT1037746] to JG. We thank Dr Rachel de las Heras for helpful suggestions and Rowan Tweedale for critically reading the manuscript, and Associate Professor Deborah Starkey for her help with CT scanning.

Competing Interests

The authors have declared that no competing interest exists.

References

- Kyriakou A, Neufeld E, Werner B, et al. A review of numerical and experimental compensation techniques for skull-induced phase aberrations in transcranial focused ultrasound. *Int J Hyperthermia* 2014; 30: 36-46.
- Hynynen K, and McDannold N. MRI guided and monitored focused ultrasound thermal ablation methods: a review of progress. *Int J Hyperthermia* 2004; 20: 725-737.
- Hynynen K, Clement GT, McDannold N, et al. 500-element ultrasound phased array system for noninvasive focal surgery of the brain: a preliminary rabbit study with ex vivo human skulls. *Magn Reson Med* 2004; 52: 100-107.
- Leinenga G, Langton C, Nisbet R, and Götz J. Ultrasound treatment of neurological diseases - current and emerging applications. *Nat Rev Neurol* 2016; 12: 161-174.
- Deng L, O'Reilly MA, Jones RM, et al. A multi-frequency sparse hemispherical ultrasound phased array for microbubble-mediated transcranial therapy and simultaneous cavitation mapping. *Phys Med Biol* 2016; 61: 8476-8501.
- Carpentier A, Canney M, Vignot A, et al. Clinical trial of blood-brain barrier disruption by pulsed ultrasound. *Sci Transl Med* 2016; 8: 343re342.
- Baseri B, Choi JJ, Deffieux T, et al. Activation of signaling pathways following localized delivery of systemically administered neurotrophic factors across the blood-brain barrier using focused ultrasound and microbubbles. *Phys Med Biol* 2012; 57: N65-81.
- Baseri B, Choi JJ, Tung YS, and Konofagou EE. Multi-modality safety assessment of blood-brain barrier opening using focused ultrasound and definity microbubbles: a short-term study. *Ultrasound Med Biol* 2010; 36: 1445-1459.
- Fan CH, Liu HL, Ting CY, et al. Submicron-bubble-enhanced focused ultrasound for blood-brain barrier disruption and improved CNS drug delivery. *PLoS One* 2014; 9: e96327.

- Choi JJ, Selert K, Gao Z, et al. Noninvasive and localized blood-brain barrier disruption using focused ultrasound can be achieved at short pulse lengths and low pulse repetition frequencies. *J Cereb Blood Flow Metab* 2011; 31: 725-737.
- Choi JJ, Feshitan JA, Baseri B, et al. Microbubble-size dependence of focused ultrasound-induced blood-brain barrier opening in mice in vivo. *IEEE Trans Biomed Eng* 2010; 57: 145-154.
- McDannold N, Vykhodtseva N, and Hynynen K. Blood-brain barrier disruption induced by focused ultrasound and circulating preformed microbubbles appears to be characterized by the mechanical index. *Ultrasound Med Biol* 2008; 34: 834-840.
- O'Reilly MA, Hough O, and Hynynen K. Blood-Brain Barrier Closure Time After Controlled Ultrasound-Induced Opening Is Independent of Opening Volume. *J Ultrasound Med* 2017; 36: 475-483.
- McDannold N, Zhang Y, and Vykhodtseva N. The Effects of Oxygen on Ultrasound-Induced Blood-Brain Barrier Disruption in Mice. *Ultrasound Med Biol* 2017; 43: 469-475.
- Choi JJ, Pernot M, Small SA, and Konofagou EE. Noninvasive, transcranial and localized opening of the blood-brain barrier using focused ultrasound in mice. *Ultrasound Med Biol* 2007; 33: 95-104.
- Choi JJ, Pernot M, Brown TR, et al. Spatio-temporal analysis of molecular delivery through the blood-brain barrier using focused ultrasound. *Phys Med Biol* 2007; 52: 5509-5530.
- Choi JJ, Selert K, Vlachos F, et al. Noninvasive and localized neuronal delivery using short ultrasonic pulses and microbubbles. *Proc Natl Acad Sci U S A* 2011; 108: 16539-16544.
- Kinoshita M, McDannold N, Jolesz FA, and Hynynen K. Noninvasive localized delivery of Herceptin to the mouse brain by MRI-guided focused ultrasound-induced blood-brain barrier disruption. *Proc Natl Acad Sci U S A* 2006; 103: 11719-11723.
- Leinenga G, and Götz J. Scanning ultrasound removes amyloid-beta and restores memory in an Alzheimer's disease mouse model. *Sci Transl Med* 2015; 7: 278ra233.
- Raymond SB, Treat LH, Dewey JD, et al. Ultrasound enhanced delivery of molecular imaging and therapeutic agents in Alzheimer's disease mouse models. *PLoS One* 2008; 3: e2175.
- Jordao JF, Ayala-Grosso CA, Markham K, et al. Antibodies targeted to the brain with image-guided focused ultrasound reduces amyloid-beta plaque load in the TgCRND8 mouse model of Alzheimer's disease. *PLoS One* 2010; 5: e10549.
- Nisbet RM, van der Jeugd A, Leinenga G, et al. Combined effects of scanning ultrasound and a tau-specific single chain antibody in a tau transgenic mouse model. *Brain* 2017; 140: 1220-1230.
- Jordao JF, Thevenot E, Markham-Coultes K, et al. Amyloid-beta plaque reduction, endogenous antibody delivery and glial activation by brain-targeted, transcranial focused ultrasound. *Exp Neurol* 2013; 248: 16-29.
- Burgess A, Dubey S, Yeung S, et al. Alzheimer disease in a mouse model: MR imaging-guided focused ultrasound targeted to the hippocampus opens the blood-brain barrier and improves pathologic abnormalities and behavior. *Radiology* 2014; 273: 736-745.
- Leinenga G, and Götz J. Safety and efficacy of scanning ultrasound treatment of aged APP23 mice. *Front Neurosci* 2018; 12: 55
- McDannold N, Vykhodtseva N, and Hynynen K. Effects of acoustic parameters and ultrasound contrast agent dose on focused-ultrasound induced blood-brain barrier disruption. *Ultrasound Med Biol* 2008; 34: 930-937.
- Hatch RJ, Leinenga G, and Götz J. Scanning Ultrasound (SUS) Causes No Changes to Neuronal Excitability and Prevents Age-Related Reductions in Hippocampal CA1 Dendritic Structure in Wild-Type Mice. *PLoS One* 2016; 11: e0164278.
- McDannold N, Arvanitis CD, Vykhodtseva N, and Livingstone MS. Temporary disruption of the blood-brain barrier by use of ultrasound and microbubbles: safety and efficacy evaluation in rhesus macaques. *Cancer Res* 2012; 72: 3652-3663.
- Downs ME, Buch A, Sierra C, et al. Long-Term Safety of Repeated Blood-Brain Barrier Opening via Focused Ultrasound with Microbubbles in Non-Human Primates Performing a Cognitive Task. *PLoS One* 2015; 10: e0125911.
- Liu HL, Jan CK, Chu PC, et al. Design and experimental evaluation of a 256-channel dual-frequency ultrasound phased-array system for transcranial blood-brain barrier opening and brain drug delivery. *IEEE Trans Biomed Eng* 2014; 61: 1350-1360.
- O'Reilly MA, Jones RM, Barrett E, et al. Investigation of the Safety of Focused Ultrasound-Induced Blood-Brain Barrier Opening in a Natural Canine Model of Aging. *Theranostics* 2017; 7: 3573-3584.
- Pernot M, Aubry JF, Tanter M, et al. In vivo transcranial brain surgery with an ultrasonic time reversal mirror. *J Neurosurg* 2007; 106: 1061-1066.
- Laure B, Petraud A, Sury F, et al. Resistance of the sheep skull after a monocortical cranial graft harvest. *J Craniomaxillofac Surg* 2012; 40: 261-265.
- Reid SJ, McKean NE, Henty K, et al. Alzheimer's disease markers in the aged sheep (*Ovis aries*). *Neurobiol Aging* 2017; 58: 112-119.
- Langton CM, Wille ML, and Flegg MB. A deconvolution method for deriving the transit time spectrum for ultrasound propagation through cancellous bone replica models. *Proc Inst Mech Eng H* 2014; 228: 321-329.

36. Hayward G, and Lewis JE. Comparison of some non-adaptive deconvolution techniques for resolution enhancement of ultrasonic data. *Ultrasonics* 1989; 27: 155-164.
37. Sin S-K, and Chen C-H. A comparison of deconvolution techniques for the ultrasonic nondestructive evaluation of materials. *Trans. Img. Proc.* 1992; 1: 3-10.
38. Madenci E, and Guven I. *The Finite Element Method and Applications in Engineering Using ANSYS®*, 2nd ed., ed., Boston, MA : Springer US : Imprint: Springer, Boston, MA; 2015.
39. Howard CQ, and Cazzolato BS. *Acoustic analyses using Matlab and Ansys*. CRC Press, Boca Raton; 2015.
40. Dual J, Hahn P, Leibacher I, et al. Acoustofluidics 19: Ultrasonic microrobotics in cavities: devices and numerical simulation. *Lab on a Chip* 2012; 12: 4010-4021.
41. Tretbar SH, Plinkert PK, and Federspil PA. Accuracy of ultrasound measurements for skull bone thickness using coded signals. *IEEE Trans Biomed Eng* 2009; 56: 733-740.
42. Teja JL, Lopez-Haro SA, Leija L, and Vera A. A finite element simulation of High Intensity Focused Ultrasound with polyacrylamide as coupling material for acoustic hemostasis. 2013 Pan American Health Care Exchanges (PAHCE). 2013
43. Zell K, Sperl JI, Vogel MW, et al. Acoustical properties of selected tissue phantom materials for ultrasound imaging. *Phys Med Biol* 2007; 52:N475-484.
44. Elias WJ, Huss D, Voss T, et al. A pilot study of focused ultrasound thalamotomy for essential tremor. *N Engl J Med* 2013; 369: 640-648.
45. Yarmolenko PS, Moon EJ, Landon C, et al. Thresholds for thermal damage to normal tissues: an update. *Int J Hyperthermia* 2011; 27: 320-343.
46. McDannold N, Vykhodtseva N, Jolesz FA, and Hynynen K. MRI investigation of the threshold for thermally induced blood-brain barrier disruption and brain tissue damage in the rabbit brain. *Magn Reson Med* 2004; 51: 913-923.
47. Marquet F, Teichert T, Wu SY, et al. Real-time, transcranial monitoring of safe blood-brain barrier opening in non-human primates. *PLoS One* 2014; 9: e84310.
48. Huang Y, Alkins R, Schwartz ML, and Hynynen K. Opening the Blood-Brain Barrier with MR Imaging-guided Focused Ultrasound: Preclinical Testing on a Trans-Human Skull Porcine Model. *Radiology* 2017; 282: 123-130.
49. Liyanage KA, Steward C, Moffat BA, et al. Development and Implementation of a Corriedale Ovine Brain Atlas for Use in Atlas-Based Segmentation. *PLoS One* 2016; 11: e0155974.
50. Polanco JC, Li C, Bodea LG, et al. Amyloid-beta and tau complexity - towards improved biomarkers and targeted therapies. *Nat Rev Neurol* 2018; 14: 22-39.
51. Tekirian TL, Cole GM, Russell MJ, et al. Carboxy terminal of beta-amyloid deposits in aged human, canine, and polar bear brains. *Neurobiol Aging* 1996; 17: 249-257.
52. Johnstone EM, Chaney MO, Norris FH, et al. Conservation of the sequence of the Alzheimer's disease amyloid peptide in dog, polar bear and five other mammals by cross-species polymerase chain reaction analysis. *Brain Res Mol Brain Res* 1991; 10: 299-305.
53. Lee SE, Hyun H, Park MR, et al. Production of transgenic pig as an Alzheimer's disease model using a multi-cistronic vector system. *PLoS One* 2017; 12: e0177933.
54. Lind NM, Moustgaard A, Jelsing J, et al. The use of pigs in neuroscience: modeling brain disorders. *Neurosci Biobehav Rev* 2007; 31: 728-751.
55. Horodyckid C, Canney M, Vignot A, et al. Safe long-term repeated disruption of the blood-brain barrier using an implantable ultrasound device: a multiparametric study in a primate model. *J Neurosurg* 2017; 126: 1351-1361.
56. Morton AJ, and Avanzo L. Executive decision-making in the domestic sheep. *PLoS One* 2011; 6: e15752.
57. Wu SY, Tung YS, Marquet F, et al. Transcranial cavitation detection in primates during blood-brain barrier opening--a performance assessment study. *IEEE Trans Ultrason Ferroelectr Freq Control* 2014; 61: 966-978.
58. Arvanitis CD, Vykhodtseva N, Jolesz F, et al. Cavitation-enhanced nonthermal ablation in deep brain targets: feasibility in a large animal model. *J Neurosurg* 2016; 124: 1450-1459.
59. Konofagou EE. Optimization of the ultrasound-induced blood-brain barrier opening. *Theranostics* 2012; 2: 1223-1237.
60. Deffieux T, and Konofagou EE. Numerical study of a simple transcranial focused ultrasound system applied to blood-brain barrier opening. *IEEE Trans Ultrason Ferroelectr Freq Control* 2010; 57: 2637-2653.
61. Wu SY, Sanchez CS, Samiotaki G, et al. Characterizing Focused-Ultrasound Mediated Drug Delivery to the Heterogeneous Primate Brain In Vivo with Acoustic Monitoring. *Sci Rep* 2016; 6: 37094.
62. Saunders NR, Dziegielewska KM, Mollgard K, and Habgood MD. Markers for blood-brain barrier integrity: how appropriate is Evans blue in the twenty-first century and what are the alternatives? *Front Neurosci* 2015; 9: 385.
63. Choi JJ, Wang S, Tung YS, et al. Molecules of various pharmacologically-relevant sizes can cross the ultrasound-induced blood-brain barrier opening in vivo. *Ultrasound Med Biol* 2010; 36: 58-67.
64. Hynynen K, McDannold N, Sheikov NA, et al. Local and reversible blood-brain barrier disruption by noninvasive focused ultrasound at frequencies suitable for trans-skull sonications. *Neuroimage* 2005; 24: 12-20.
65. Pinton G, Aubry JF, Bossy E, et al. Attenuation, scattering, and absorption of ultrasound in the skull bone. *Med Phys* 2012; 39: 299-307.
66. McDannold N, King RL, and Hynynen K. MRI monitoring of heating produced by ultrasound absorption in the skull: in vivo study in pigs. *Magn Reson Med* 2004; 51: 1061-1065.